Effect of internal electric field on InAs/GaAs quantum dot solar cells

Kasamatsu, Naofumi
Kada, Tomoyuki
Hasegawa, Aiko
Harada, Yukihiro
Kita, Takashi

(Citation)
Journal of Applied Physics,115:083510-083510

(Issue Date)
2014

(Resource Type)
journal article

(Version)
Version of Record

(URL)
https://hdl.handle.net/20.500.14094/90002575

Effect of internal electric field on InAs/GaAs quantum dot solar cells

Naofumi Kasamatsu, Tomoyuki Kada, Aiko Hasegawa, Yukihiro Harada, and Takashi Kita

Citation: Journal of Applied Physics **115**, 083510 (2014); doi: 10.1063/1.4867042
View online: http://dx.doi.org/10.1063/1.4867042
View Table of Contents: http://scitation.aip.org/content/aip/journal/jap/115/8?ver=pdfcov
Published by the AIP Publishing

Effect of internal electric field on InAs/GaAs quantum dot solar cells

Naofumi Kasamatsu, Tomoyuki Kada, Aiko Hasegawa, Yukihiro Harada, and Takashi Kita
Department of Electrical & Electronic Engineering, Graduate School of Engineering, Kobe University, 1-1 Rokkodai, Nada, Kobe 657-8501, Japan

(Received 2 October 2013; accepted 15 February 2014; published online 26 February 2014)

We studied time-resolved carrier recombination in InAs/GaAs quantum dot (QD) solar cells. The electric field in a *p-i-n* diode structure spatially separates photoexcited carriers in QDs, strongly affecting the conversion efficiency of intermediate-band solar cells. The radiative decay lifetime is dramatically reduced in a strong electric field (193 kV/cm) by efficient recombination due to strong carrier localization in each QD and significant tunneling-assisted electron escape. Conversely, an electric field of the order of 10 kV/cm maintains electronic coupling in the stacked QDs and diminishes tunneling-assisted electron escape. © *2014 AIP Publishing LLC*.
[http://dx.doi.org/10.1063/1.4867042]

I. INTRODUCTION

Achieving an energy conversion efficiency of more than 50% is strongly demanded for next generation solar cells (SCs). Generally, for single-junction SCs, the conversion efficiency is limited mainly by the transmission loss and thermalization loss.[1–3] Therefore, the maximum conversion efficiency is obtained for an optimum band gap energy called the Shockley–Queisser limit.[1] In particular, various device structures have been proposed for reducing the transmission loss. Multijunction SCs are one of the most promising structures; they consist of tandem heterostructures of semiconductors with different band-gap energies, where transmitted light passing through a wider-gap semiconductor is absorbed in a narrower-gap material placed at the back. The highest conversion efficiency of a multijunction SC is currently 44.4%, which was realized using a triple-junction structure of InGaP, GaAs, and InGaAs.[4] Another promising structure that is expected to dramatically reduce the transmission loss is intermediate-band (IB) SCs.[5] An IB placed in the band gap of a host semiconductor plays a key role in extra photoabsorption. If photoexcitation provides a quick pass to the conduction band for electrons pumped from the valence band to the IB, extra photocurrent is generated. A single IB in a band gap creates three types of optical transitions; therefore, an extremely high energy conversion efficiency, comparable to that of multijunction SCs, is expected. The optimum conversion efficiency of IBSC is 48% under one-sun irradiation and 68% under the maximum concentration of solar irradiance.[6] Here, the optical transition probability from the IB to the conduction band should be sufficiently strong for electrons in the IB. Since low-dimensional confinement structures relax the optical selection rule for the intraband transition from the quantized states to the extended conduction band, lower-dimensional structures yield stronger intraband photoabsorption. Thus, quantized states formed in three-dimensionally confined quantum dots (QDs) have been extensively explored for realizing IBSCs.[7–16]

Recently, we performed theoretical calculations for the effects of the absorption coefficients on the conversion efficiency of InAs/GaAs QD-IBSCs.[17] The conversion efficiency strongly depends on the relative absorption coefficients between the interband and intraband transitions. If we assume an interband absorption coefficient of 40 000 cm^{-1}, an intraband absorption coefficient of 1000 cm^{-1} ensures a conversion efficiency of 40%, and 30 000 cm^{-1} is reportedly essential for achieving 50% efficiency.[17] Recent theoretical calculations and experiments have demonstrated that the intraband absorption coefficient in InAs/GaAs QDs is on the order of several hundred per centimeter.[18,19] The earlier theoretical calculations[5,17] ignored carrier escape from the IB. However, tunneling and thermal carrier escape reduce the extra photocurrent generation in IBSCs and lower the open circuit voltage.[8,10,12,16] In this work, we studied the effects of the internal electric field on the carrier wavefunctions and tunneling-assisted carrier escape in InAs/GaAs QD-IBSCs using time-resolved photoluminescence (PL) measurements. To focus on the effects of the electric field, here, we studied the optical responses at low temperature, which provides a condition we can ignore the thermal carrier escape process. The electric field sensitively modifies the coupled electronic states in closely stacked QDs and influences the emission wavelength, intensity, and radiative decay lifetime.

II. InAs/GaAs QDSCs AND EXPERIMENTAL

InAs/GaAs QDSC structures were grown on n^+-GaAs(001) substrates using solid-source molecular beam epitaxy. Detailed sample structures used in this study are listed in Table I. An undoped nine-stacked InAs/GaAs QD layer was grown at 480 °C on a buffer layer of *i*-GaAs(1)/*n*-GaAs/n^+-GaAs grown at 550 °C. The nominal thickness of the deposited InAs was 0.61 nm [2.0 monolayers (MLs)], and the As flux during the QD growth was 1.3×10^{-3} Pa. The GaAs spacer layer thickness was 5.1 nm (18 ML). A typical transmission electron microscope (TEM) image of the nine-stacked QDs is shown in Fig. 1. QDs were closely stacked along the growth direction so that the electronic states in the stacked QDs couple with each other.[20,21] Subsequently, p^+-GaAs/*p*-AlGaAs/*p*-GaAs/*i*-GaAs(2) layers were deposited on the stacked QD layers. The *p* layers were deposited at 500 °C and the *i*-GaAs layer was at 480 °C. The

TABLE I. Detailed sample structures.

	Reference QDs	SC at 46 kV/cm		SC at 193 kV/cm	
	Thickness (nm)	Thickness (nm)	Carrier concentration (cm^{-3})	Thickness (nm)	Carrier concentration (cm^{-3})
p^+-GaAs	…	50	Be: 1×10^{19}	50	Be: 1×10^{19}
p-AlGaAs	…	50	Be: 2×10^{18}	50	Be: 2×10^{18}
p-GaAs	…	150	Be: 2×10^{18}	350	Be: 2×10^{18}
i-GaAs(2)	100	209.4	…	9.4	…
9 period of InAs-QD layer		GaAs spacer layer thickness: 5.1 nm (18 ML), Nominal thickness of InAs: 0.61 nm (2.0 ML)			
i-GaAs(1)	400	44	…	14.5	…
n-GaAs	…	700	Si: 5×10^{17}	1000	Si: 1×10^{17}
n^+-GaAs	…	150	Si: 1×10^{18}	150	Si: 1×10^{18}
Substrate	Undoped GaAs(001)	n^+-GaAs(001)		n^+-GaAs(001)	

built-in electric field in the intrinsic layer was controlled by changing the thicknesses of the i-GaAs(1) and i-GaAs(2) layers. The expected internal electric fields applied to the QDs were 46 and 193 kV/cm when the total intrinsic layer thicknesses were 299.3 and 69.8 nm, respectively. For a reference sample, we provided nine-stacked QDs grown on an undoped GaAs(001) substrate. The capping layer thickness of the GaAs in the reference sample was 100 nm. Although the built-in internal electric field of this reference sample was not zero in a strict sense, we refer to it as a reference sample with a very small internal electric field.

PL measurements were conducted through excitation using a laser diode with a wavelength of 659 nm. Time-resolved PL measurements were performed by using a near-infrared streak camera system with a temporal resolution of 20 ps. The light source used was a mode-locked Ti:sapphire pulse laser with wavelengths of 800 and 900 nm. The repetition rate was 4 MHz. These experiments were conducted under a short circuit condition to avoid photoinduced changes in the internal electric field of the SCs.

III. RESULTS AND DISCUSSION

Figure 2 shows the PL spectra measured at 16 K. As the electric field increased, the PL peak wavelength exhibited an obvious red shift; moreover, the PL intensity decreases dramatically. These are typical features of the quantum-confined Stark effect (QCSE); the energy potential of the QDs is electrically deformed by the electric field, and the electron and hole wavefunctions are spatially separated in the confined potential. Here, we investigated the in-plane linear polarization characteristics of the PL. The reference sample and the SC at 46 kV/cm exhibit obvious linear polarization anisotropy; the [−110]-polarization component is stronger than the [110] component. This is direct evidence of valence-band mixing in stacked QDs where the electronic states are coupled electronically along the stacking direction.[20,21] This anisotropy originally comes from the anisotropic QD shape and the piezoelectricity caused by the strain field.[20,22] Conversely, the SC at 193 kV/cm does not show

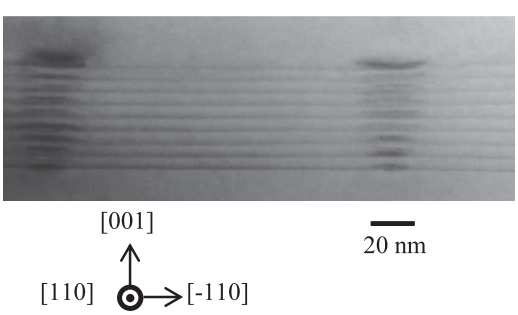

FIG. 1. (110)-cross-sectional TEM image of nine-stacked InAs/GaAs QDs with the GaAs spacer layer thickness of 5.1 nm.

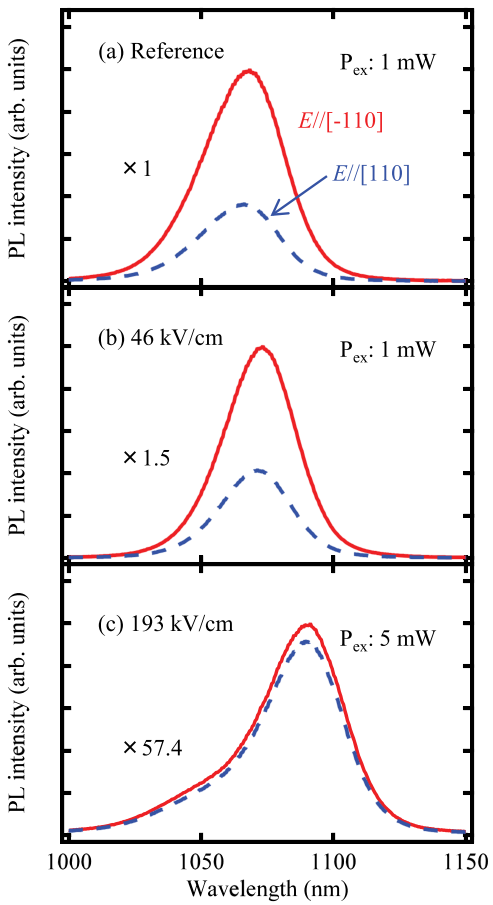

FIG. 2. In-plane linear PL-polarization anisotropy of QDs using laser diode with the wavelength of 659 nm at 16 K for (a) a reference sample and SCs at (b) 46 and (c) 193 kV/cm. Solid and dashed lines indicate results for the [–110] and [110] polarizations, respectively. The excitation powers for (a), (b), and (c) were 1, 1, and 5 mW, respectively.

TABLE II. Thermal activation energies estimated from the temperature dependence of the PL intensity.

	Thermal activation energies (meV)	
Electric field (kV/cm)	ΔE_1	ΔE_2
~0	187	68
46	175	67
193	58	13

such polarization anisotropy. This indicates that electronic coupling along the stacking direction becomes weak under the strong electric field. Therefore, the electronic states are localized in each QD. This strong vertical confinement diminishes the anisotropy.

We investigated the thermal activation energy of carriers by analyzing the thermal quenching of the PL intensity using a model considering two activation energies. The evaluated thermal activation energies are summarized in Table II. ΔE_1 and ΔE_2 are attributed to the activation energies from the ground state in QDs to the GaAs band edge and the excited state, respectively. The activation energy decreases as the internal electric field increases. In particular, the reduction for the SC at 193 kV/cm was remarkable. This indicates that the electric field lowers the confining potential barrier. The reduced potential barrier height also enhances tunneling-assisted carrier escape and diminishes the open circuit voltage of the SC.

Next, to clarify the influence of the internal electric field on the carrier recombination process, we performed time-resolved PL measurements. The excitation laser wavelength was 800 nm, which provides excitation above the GaAs barrier. Figure 3 displays the detection wavelength dependence of the PL decay profile measured at 3 K. The reference sample shows a slow single exponential decay and clear detection wavelength dependence. The PL decay time was approximately 2 ns. Since the decay time of conventional single-layer InAs/GaAs QDs is approximately 1 ns,[23,24] the slow decay is attributed to delocalization of the exciton wavefunction in the stacked, coupled QDs. The detection wavelength dependence of the PL decay time of QDs with inhomogeneous size distribution has been widely studied during the past decade.[25,26] Generally, the detection wavelength dependence is small at low temperature and becomes obvious at elevating temperature. The detection wavelength dependence obviously observed at this low temperature indicates spatial carrier transfer along the stacking direction, which has never been observed in single-layer QDs. On the other hand, the SC at 46 kV/cm shows a double exponential decay. The rapid initial decay is slightly shorter than 2 ns, and the following slow decay becomes longer than 2 ns. The internal electric field spatially separates electrons and holes toward the opposite directions along the stacked QDs. Thus, the double exponential decay comprises exciton recombination before and after the field-induced spatial wavefunction localization. The detection wavelength dependence of this slow decay component indicates that the electronic states still extend along the stacking direction under this internal electric field.

Figures 4(a) and 4(b) show the temperature dependence of the PL decay profile of the reference sample and the SC at 46 kV/cm, respectively. Here, we used a pulse laser with the wavelength of 900 nm to avoid carrier relaxation from the GaAs barrier. The below barrier excitation enables us to perform precise analysis of carrier dynamics reflecting the translational motion. With increasing temperature, the decay time of the reference sample increased monotonically. This change is caused by translational motion of carriers in the coupled QDs.[27] In contrast to uncoupled, isolated conventional QDs, coupled QDs cause valence-band mixing, as mentioned above, which reduces the hole mass of the fundamental state. Then, both electrons and holes can move along the stacking direction. Incidentally, as summarized in Fig. 4(c), the decay time starts to increase above ~30 K. The appearance of a threshold in the temperature dependence of the radiative decay time indicates the presence of a threshold in the homogeneous linewidth producing the electronic coupling; the inhomogeneously distributed energy states within the homogeneous energy width can couple with each other.[21]

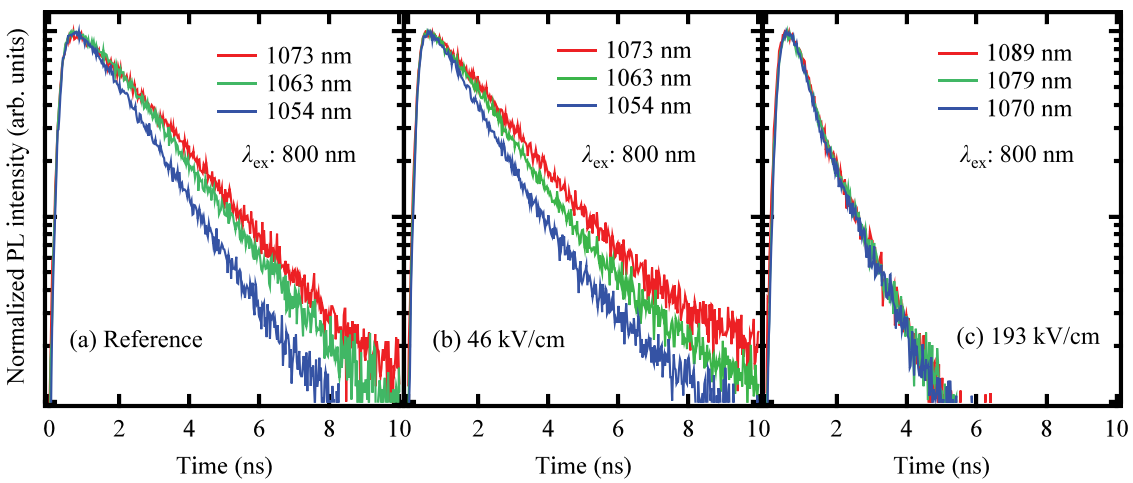

FIG. 3. Detection wavelength dependence of PL decay profile measured at 3 K for (a) a reference sample and SCs at (b) 46 and (c) 193 kV/cm. The excitation laser wavelength was 800 nm, which provides excitation above the GaAs barrier. The excitation powers for (a), (b), and (c) were 100, 100, and 250 μW, respectively.

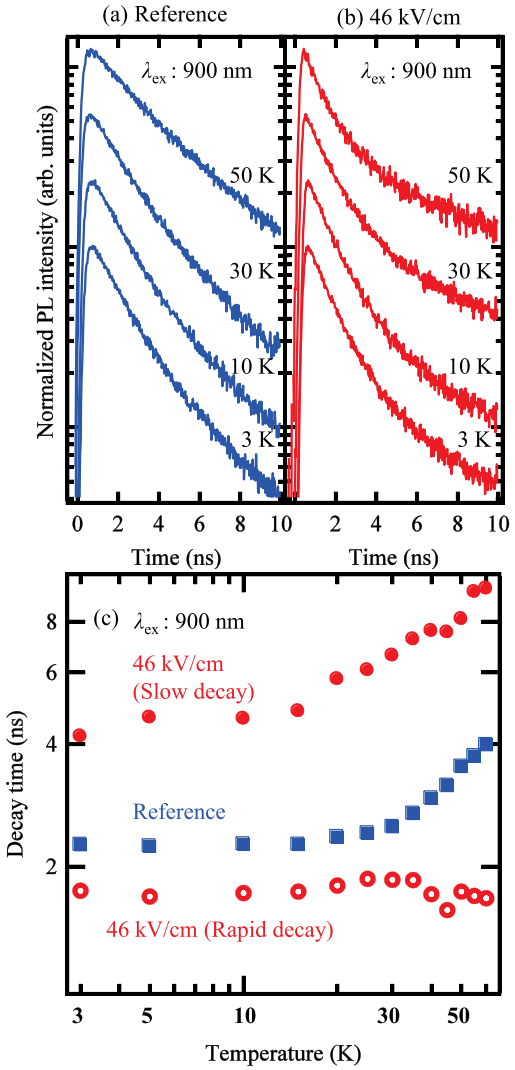

FIG. 4. Temperature dependence of PL-decay profile for (a) a reference sample and (b) SC at 46 kV/cm, and (c) their temperature dependence of analysed PL-decay times. The excitation wavelength of 900 nm was used to avoid carrier relaxation from the GaAs barrier. The detection wavelengths for (a) and (b) are the PL-peak wavelengths of each spectrum. The excitation powers for (a) and (b) were 300 and 330 μW, respectively.

This process is discussed in detail in Ref. 21. Conversely, the rapid decay component observed in the SC at 46 kV/cm was almost independent of the temperature. The following slower decay shows a clear temperature dependence reflecting the spatial carrier motion in the coupled QDs. These results demonstrate that an internal electric field of the order of 10 kV/cm maintains electronic coupling in the stacked QDs.

For an extremely large internal electric field, we observed a quite different PL decay profile as shown in Fig. 3(c). The decay was very fast and can be described by double exponential components of τ_1 and τ_2 ($\tau_1 < \tau_2$). Moreover, the detection wavelength dependence of the PL decay disappeared, which indicates that the field-induced decoupled energy states in QDs prohibit the spatial carrier transfer at the low temperature. A strong electric field of 193 kV/cm causes apparent QCSE such as the PL-intensity reduction and the red shift of the PL peak, as shown in Fig. 2. The recombination rate of electrons and holes should become greater in the decoupled QDs. The decay time τ_2 was 1.09 ns, which is close to a typical PL decay time in conventional single-layer QDs.[23,24] Moreover, the hole mass of the fundamental state becomes large owing to the electric-field-induced decoupling of the electronic states in the stacked QDs. The hole quantization in the decoupled QDs becomes weaker than the electron's one, and, therefore, the strong electric field can easily extract electrons from the QDs; in other words, tunneling-assisted electron escape occurs easily. The electron escape rapidly reduces the PL intensity with a time constant τ_1 of 0.46 ns. This short lifetime in the high electric field will prevent photoexcitation of electrons in the IB in QDs, and the open circuit voltage of this SC eventually becomes small. To confirm the tunneling effect in the SC, we measured the external quantum efficiency (EQE). Figures 5(a) and 5(b) show EQE spectra near the infrared wavelength region indicating the optical response of the QDs measured at 12 K and room temperature, respectively. The EQE spectra are compared with unpolarized PL spectra of the QDs in Figs. 5(c) and 5(d) to clarify contribution of the QD states to the EQE signal. The continuously extending significant EQE signal from the QD states toward the GaAs-band edge is attributed to the electronic states of the wetting layer (WL). It is noted that the EQE at 12 K depends on the electric field; the EQE of the SC at 193 kV/cm is larger than that of the cell at 46 kV/cm. Since the thermal process is suppressed at the low temperature, the increased EQE is attributed to tunneling-assisted electron extraction. Conversely, the EQE at room temperature was almost identical except for the wavelength region of the QD-PL band. This indicates that thermal electron escape from the shallower WL states becomes remarkable rather than the QD states. Efficient two-step photoexcitation in IBSCs is achieved by suppressing both the tunneling and thermal electron escape processes. According to this work, tunneling electron escape turned out

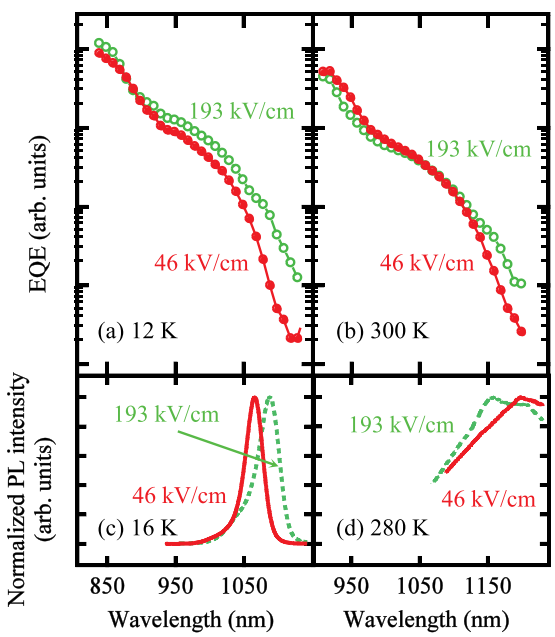

FIG. 5. EQE spectra in the near-infrared region measured at (a) 12 and (b) 300 K. Solid and open circles indicate results for SCs at 46 and 193 kV/cm, respectively. PL spectra at (c) 16 and (d) 280 K. Solid and dashed lines indicate results for SCs at 46 and 193 kV/cm, respectively.

to be suppressed at the built-in electric field of 46 kV/cm, which still maintains electronic coupling in stacked QDs.

In the above discussion, we considered the contribution of the built-in electric field on the electronic coupling and carrier escape from QDs. However, when sunlight shines on SCs with an external load, the built-in electric field of SCs decreases from that at the short circuit condition. When the electric field at *the maximum power point* of IBSCs satisfies the order of 10 kV/cm, two-step photoexcitation will be accomplished before electrons escape. Although the influence of the electric field on IBSCs became clear in this work, the thermal electron escape process taking over the field-assisted tunneling process at room temperature must be taken into account, in particular, for the shallower WL states, which, of course, decreases photocurrent generated by the two-step photoexcitation. Moreover, thermal electron escape from the WL states will lower the quasi-Fermi level, and, therefore, the output voltage becomes small. In order to reduce such thermal effects, further optimization of the QD structure with a moderately deep intermediate state[28] and a low density of states of the WL state[29] are necessary, which will finally realize efficient two-step photoexcitation.

IV. SUMMARY

We investigated electron recombination in InAs/GaAs QDSCs. The electric field in the *p-i-n* diode structure influences the recombination process. As the internal electric field increases, apparent QCSE such as the PL-intensity reduction and the PL-peak red shift appears. The electric field lowers the potential barrier of the QDs, and the thermal activation energy decreases as the internal electric field increases. An electric field of 46 kV/cm maintains electronic coupling in closely stacked QDs. On the other hand, an electric field of 193 kV/cm localizes the electrons and holes in each QD, and significant tunneling-assisted electron escape occurs, which prevents efficient two-step photoexcitation in IBSCs. We demonstrated that an electric field of the order of 10 kV/cm maintains electronic coupling in the stacked QDs in addition to diminishing tunneling-assisted electron escape, which is a desirable effect for IBSCs.

ACKNOWLEDGMENTS

This work was partially supported by the "Nanotechnology Network Project of the Ministry of Education, Culture, Sports, Science and Technology (MEXT), Japan" at the Research Center for Ultrahigh Voltage Electron Microscopy in Osaka University, the Incorporated Administrative Agency New Energy and Industrial Technology Development Organization (NEDO) through the funding of a new generation of concentrator photovoltaic cells, modules and systems (NGCPV) EUROPE-JAPAN, and the Ministry of Economy, Trade, and Industry (METI), Japan. The authors thank Dr. E. Taguchi and Professor H. Yasuda at Osaka University for TEM measurement.

[1]W. Shockley and H. J. Queisser, J. Appl. Phys. **32**, 510 (1961).
[2]L. C. Hirst and N. J. Ekins-Daukes, Prog. Photovolt: Res. Appl. **19**, 286 (2011).
[3]A. Luque, J. Appl. Phys. **110**, 031301 (2011).
[4]See http://sharp-world.com/corporate/news/130614.html for Press Release, Sharp Corporation (14 June 2013), accessed on 1 October 2013.
[5]A. Luque and A. Martí, Phys. Rev. Lett. **78**, 5014 (1997).
[6]T. Kita, *Energy Conversion Efficiency of Solar Cells* (CORONA, Tokyo, 2012), p. 87 (in Japanese).
[7]A. Martí, E. Antolín, C. R. Stanley, C. D. Farmer, N. López, P. Díaz, E. Cánovas, P. G. Linares, and A. Luque, Phys. Rev. Lett. **97**, 247701 (2006).
[8]A. Martí, N. López, E. Antolín, E. Cánovas, A. Luque, C. R. Stanley, C. D. Farmer, and P. Díaz, Appl. Phys. Lett. **90**, 233510 (2007).
[9]S. Tomić, T. S. Jones, and N. M. Harrison, Appl. Phys. Lett. **93**, 263105 (2008).
[10]S. M. Hubbard, C. D. Cress, C. G. Bailey, R. P. Raffaelle, S. G. Bailey, and D. M. Wilt, Appl. Phys. Lett. **92**, 123512 (2008).
[11]R. Oshima, A. Takata, and Y. Okada, Appl. Phys. Lett. **93**, 083111 (2008).
[12]Y. Okada, R. Oshima, and A. Takata, J. Appl. Phys. **106**, 024306 (2009).
[13]G. Jolley, H. F. Lu, L. Fu, H. H. Tan, and C. Jagadish, Appl. Phys. Lett. **97**, 123505 (2010).
[14]S. Tomić, Phys. Rev. B **82**, 195321 (2010).
[15]Y. Okada, T. Morioka, K. Yoshida, R. Oshima, Y. Shoji, T. Inoue, and T. Kita, J. Appl. Phys. **109**, 024301 (2011).
[16]Y. Shoji, K. Akimoto, and Y. Okada, J. Phys. D: Appl. Phys. **46**, 024002 (2013).
[17]W. G. Hu, T. Inoue, O. Kojima, and T. Kita, Appl. Phys. Lett. **97**, 193106 (2010).
[18]A. Luque, A. Martí, A. Mellor, D. F. Marrón, I. Tobías, and E. Antolín, Prog. Photovolt: Res. Appl. **21**, 658 (2013).
[19]Y. Harada, T. Maeda, and T. Kita, J. Appl. Phys. **113**, 223511 (2013).
[20]Y. Ikeuchi, T. Inoue, M. Asada, Y. Harada, T. Kita, E. Taguchi, and H. Yasuda, Appl. Phys. Express **4**, 062001 (2011).
[21]A. Takahashi, T. Ueda, Y. Bessho, Y. Harada, T. Kita, E. Taguchi, and H. Yasuda, Phys. Rev. B **87**, 235323 (2013).
[22]M. Usman, T. Inoue, Y. Harada, G. Klimeck, and T. Kita, Phys. Rev. B **84**, 115321 (2011).
[23]T. Kita, T. Maeda, and Y. Harada, Phys. Rev. B **86**, 035301 (2012).
[24]T. Kita, R. Hasegawa, and T. Inoue, J. Appl. Phys. **110**, 103511 (2011).
[25]O. Kojima, H. Nakatani, T. Kita, O. Wada, K. Akahane, and M. Tsuchiya, J. Appl. Phys. **103**, 113504 (2008).
[26]O. Kojima, H. Nakatani, T. Kita, O. Wada, and K. Akahane, J. Appl. Phys. **107**, 073506 (2010).
[27]C. F. Klingshirn, *Semiconductor Optics* (Springer-Verlag, 2007).
[28]E. Antolín, A. Martí, C. D. Farmer, P. G. Linares, E. Hernández, A. M. Sánchez, T. Ben, S. I. Molina, C. R. Stanley, and A. Luque, J. Appl. Phys. **108**, 064513 (2010).
[29]F. K. Tutu, P. Lam, J. Wu, N. Miyashita, Y. Okada, K.-H. Lee, N. J. Ekins-Daukes, J. Wilson, and H. Liu, Appl. Phys. Lett. **102**, 163907 (2013).